

1 **Epigenome-associated phenotypic acclimatization to ocean acidification in**
2 **a reef-building coral**

3 Yi Jin Liew¹, Didier Zoccola², Yong Li¹, Eric Tambutte², Alexander A. Venn², Craig T.
4 Michell¹, Guoxin Cui¹, Eva S. Deutekom³, Jaap A. Kaandorp³, Christian R. Voolstra¹,
5 Sylvain Forêt^{4†}, Denis Allemand², Sylvie Tambutte², Manuel Aranda^{1*}

6 **Affiliations:**

7 ¹King Abdullah University of Science and Technology (KAUST), Red Sea Research Center
8 (RSRC), Biological and Environmental Sciences & Engineering Division (BESE), Thuwal,
9 Saudi Arabia.

10 ²Centre Scientifique de Monaco, Marine Biology Department, Principality of Monaco.

11 ³Computational Science Lab, Faculty of Science, University of Amsterdam, Amsterdam, The
12 Netherlands.

13 ⁴Research School of Biology, Australian National University, Canberra, Australia

14 *Correspondence to: manuel.aranda@kaust.edu.sa (M.A.)

15 †Passed away 17 December 2016

16 **Keywords:** Epigenetics, DNA methylation, coral reef, cnidarian, ocean acidification.

17

18 **Word count:** 216 (summary paragraph), 1,626 words (main text).

19 **References:** 30 (main text), 20 (Supplementary).

20 **Figures:** 4 (main text), 7 (Extended Data).

21 **Tables:** 0 (main text), 1 (Extended Data), 9 (Supplementary Data)

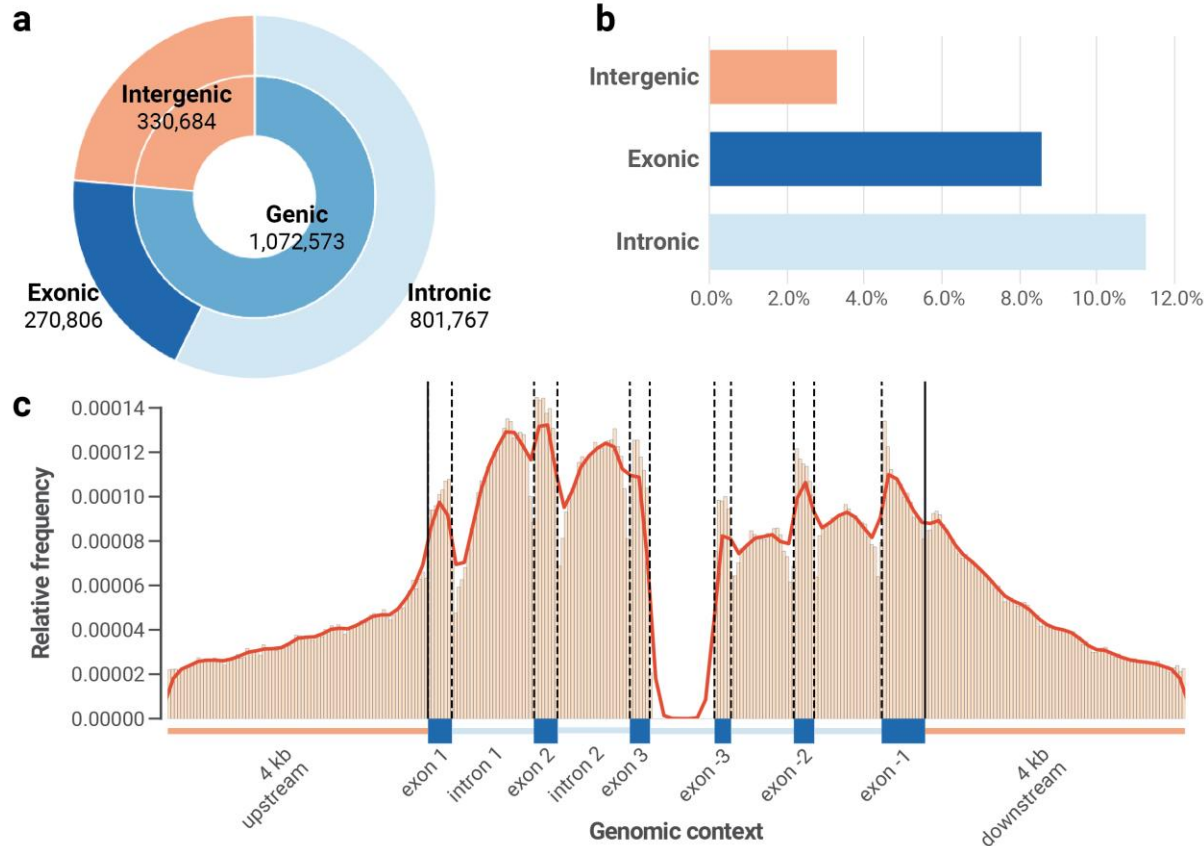
22 **Over the last century, the anthropogenic production of CO₂ has led to warmer**
23 **(+0.74 °C) and more acidic (-0.1 pH) oceans¹, resulting in increasingly frequent and**
24 **severe mass bleaching events worldwide that precipitate global coral reef decline^{2,3}. To**
25 **mitigate this decline, proposals to augment the stress tolerance of corals through genetic**
26 **and non-genetic means have been gaining traction⁴. Work on model systems has shown**
27 **that environmentally induced alterations in DNA methylation can lead to phenotypic**
28 **acclimatization^{5,6}. While DNA methylation has been observed in corals⁷⁻¹⁰, its potential**
29 **role in phenotypic plasticity has not yet been described. Here, we show that, similar to**
30 **findings in mice¹¹, DNA methylation significantly reduces spurious transcription in the**
31 **Red Sea coral *Stylophora pistillata*, suggesting the evolutionary conservation of this**
32 **essential mechanism in corals. Furthermore, we find that DNA methylation also reduces**
33 **transcriptional noise by fine-tuning the expression of highly expressed genes. Analysis**
34 **of DNA methylation patterns of corals subjected to long-term pH stress showed**
35 **widespread changes in pathways regulating cell cycle and body size. Correspondingly,**
36 **we found significant increases in cell and polyp sizes that resulted in more porous**
37 **skeletons, supporting the maintenance of linear extension rates under conditions of**
38 **reduced calcification. These findings suggest an epigenetic component in phenotypic**
39 **acclimatization, providing corals with an additional mechanism to cope with climate**
40 **change.**

41 *Stylophora pistillata* is a globally distributed scleractinian coral with an available draft
42 genome (Voolstra et al., 2017, under review). Previous work has demonstrated its plasticity
43 and resilience in the face of high pCO₂ conditions^{12,13}. Remarkably, this coral remains
44 capable of calcifying in seawater with significantly reduced pH of 7.2 even when aragonite,
45 the main component of coral skeletons, falls below its saturation point in seawater (i.e.,
46 $\Omega_{\text{aragonite}} < 1$)¹³. Previous work showed that the linear extension rate of *S. pistillata* in acidic

47 seawater is not significantly different from that measured under control conditions (pH 8.0)
48 despite the significantly reduced calcification rates¹².

49 To investigate whether epigenetic mechanisms regulate phenotypic acclimatization to long-
50 term pH stress, we cultivated *S. pistillata* colonies *in aquaria* for more than two years under
51 four experimental conditions of seawater pH at 7.2, 7.4, 7.8 and 8.0 (control). Conditions in
52 these aquaria were identical, except for the pCO₂ and resulting differences in carbon
53 chemistry in the tanks (3792, 2257, 856 and 538 μ atm, respectively). We performed whole
54 genome bisulphite sequencing on three replicate nubbins per tank and obtained data from
55 98% of all CpGs in the genome with a per-sample, per-position mean coverage of \sim 25 \times
56 (Supplementary Discussion 1, Supplementary Data 1).

57 The *S. pistillata* genome is sparsely methylated (1,406,097 bp, 7% of all CpGs), similar to
58 other invertebrates, e.g., 1% in the bee *Apis mellifera*¹⁴; 2% in the wasp *Nasonia*
59 *vitripennis*¹⁵; and 9% in the sea anemone *Nematostella vectensis*¹⁶. Like other invertebrates,
60 the vast majority of cytosine methylation in *S. pistillata* occurs in genic (76.2%) rather than
61 intergenic (22.9%) regions. Surprisingly, methylation in introns was higher than that in exons
62 (Fig. 1a, 1b), unlike other invertebrates where introns have been reported to have low
63 methylation^{15,16}.



64

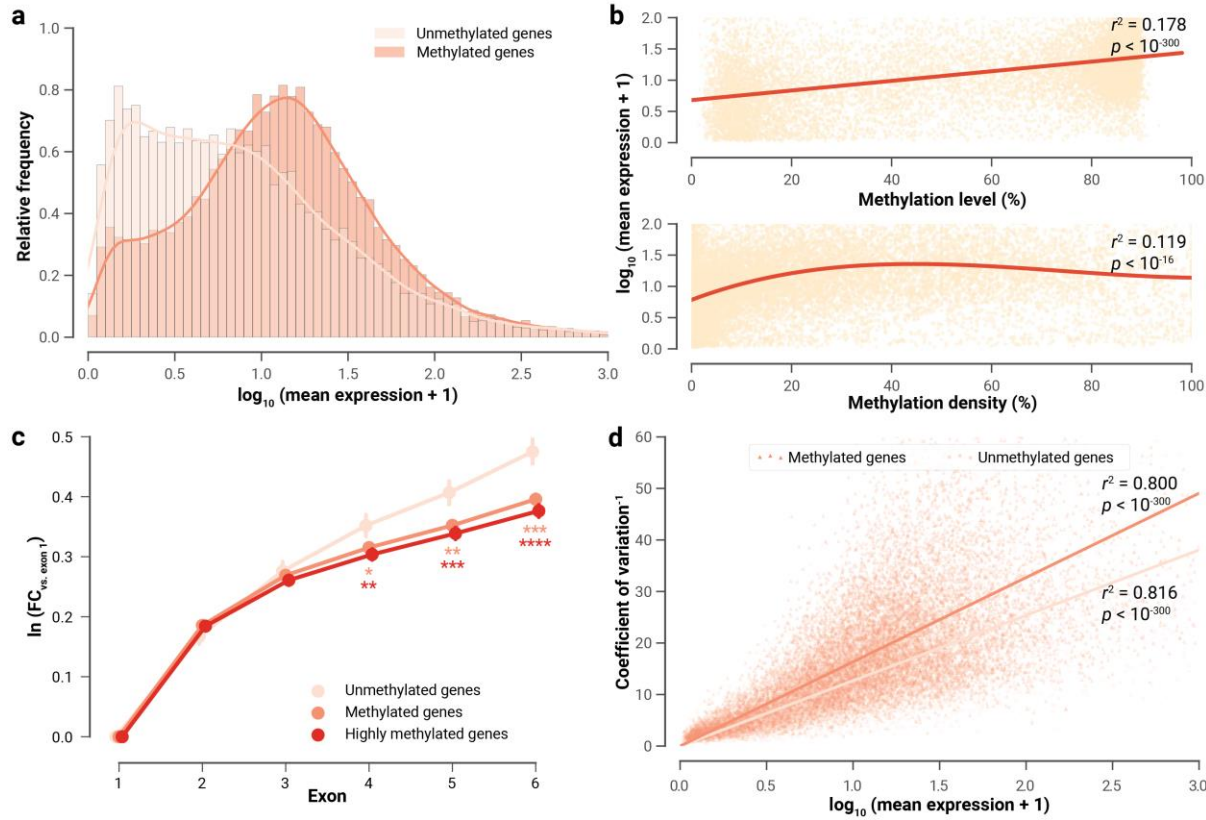
65 **Figure 1: Epigenetic landscape of *S. pistillata*.** (a) More than half of all methylated
66 positions in *S. pistillata* are located in annotated introns. (b) Introns have proportionally more
67 methylated positions (11.3%) than exons (8.6%) or intergenic regions (3.3%) even when
68 accounting for the different amounts of CpG dinucleotides in the respective regions. (c)
69 Relative frequencies of methylated positions across a standardised gene model with flanking
70 4 kb regions. Solid lines depict transcriptional start site (left) and transcription termination
71 site (right). Exons and introns in the plot have normalised lengths that correspond to their
72 respective mean lengths in *S. pistillata* (from left to right: 373 bp, 1,258 bp, 363 bp, 1,114 bp,
73 302 bp; 253 bp, 967 bp, 312 bp, 1,037 bp, 669 bp).

74

75 In contrast to vertebrates, methylation in the promoter regions of *S. pistillata* is scarce and
76 does not seem to affect gene expression (see Supplementary Discussion 2); methylated

77 positions are instead predominantly located within gene bodies (Figure 1c). Gene body
78 methylation has recently been shown, in mice, to be established via crosstalk between the
79 transcriptional machinery and histone modifications. RNA polymerase II-mediated
80 transcription establishes new methylated positions along the gene body through the action of
81 SetD2, H3K36Me3 and Dnmt3b. Methylation, in turn, reduces spurious transcription from
82 cryptic promoters within these gene bodies¹¹. Analyses of our RNA-seq data strongly indicate
83 that these functions are conserved in corals. We find that gene body methylation increases
84 with gene expression in *S. pistillata* (Fig. 2a, b), similar to other corals^{7,8}. More importantly,
85 we observe that methylated genes show significantly lower levels of spurious transcription
86 relative to unmethylated genes (Fig. 2c). Furthermore, consistent with the repressive nature of
87 methylation on expression, our analysis indicates that methylation in gene bodies also
88 reduces transcriptional noise (lower variability of gene expression levels), echoing previous
89 reports in corals and other organisms^{7,17} (Fig. 2d, Supplementary Discussion 3). These
90 findings also suggest that the biological functions of gene body methylation are likely
91 conserved across Metazoa, if at all present in the organism.

92



93

94 **Figure 2: Effect of gene body methylation on genic expression.** (a) The expression of
 95 methylated genes is significantly higher than that of unmethylated genes ($p < 10^{-300}$,
 96 Student's *t*-test). (b) Expression values for methylated genes are exponentially proportional to
 97 methylation level; however, the relationship of expression to methylation density is non-
 98 linear. Methylation density at low levels is exponentially proportional to expression values,
 99 but it plateaus at ~40%. (c) Expression levels of the first six exons were calculated as natural
 100 logarithms of fold changes relative to the expression of the first exon. The difference in
 101 expression levels is likely driven by the reduction of cryptic transcription initiation in
 102 methylated genes. The difference is greater in highly methylated genes (median methylation
 103 level $> 80\%$). Asterisks represent p values from *t*-tests of methylated (orange) or highly
 104 methylated genes (red) against unmethylated genes (peach), and coloured accordingly. *: $p <$
 105 0.05; **: $p < 0.01$; ***: $p < 0.001$; ****: $p < 0.0001$. (d) There is a linear relationship
 106 between the inverse of the coefficient of variation (cv^{-1}) and the \log_{10} -transformed mean

107 expression values from all samples. The coefficient of variation, defined as the standard
108 deviation of measured expression values divided by their mean, is consistently lower in
109 methylated genes than unmethylated genes.

110

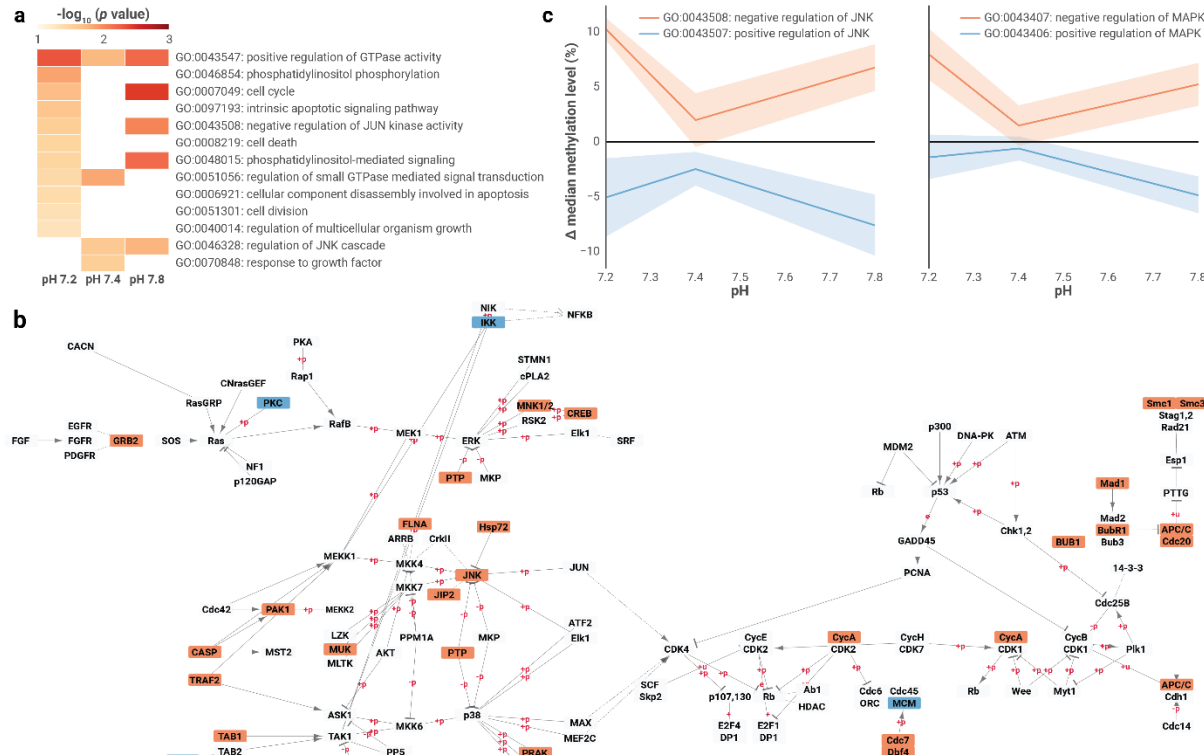
111 Based on these findings, we sought to further elucidate the potential role DNA methylation in
112 phenotypic acclimation. Using generalised linear models (GLMs), we identified genes that
113 undergo differential methylation in response to pH treatment (Supplementary Data 2). In
114 general, we observed a significant increase in overall DNA methylation with decreasing pH,
115 echoing similar observations in *Pocillopora damicornis*⁹. To validate these changes in
116 methylation, we performed amplicon-specific bisulphite sequencing of selected genes on the
117 original samples, as well as on samples of an independent experiment. These analyses
118 showed high correlation of results obtained from whole genome and amplicon-specific
119 bisulphite sequencing ($r^2 > 0.8$, $p < 0.01$, Extended Data Fig. 5a) and further confirmed a
120 high degree of reproducibility of DNA methylation changes across independent experiments
121 ($p < 0.01$, Extended Data Fig. 5b). Analyses on laser-microdissected oral and aboral tissues
122 further highlighted that most of the selected genes displayed strong and consistent tissue-
123 specific methylation patterns, similar to findings in vertebrates¹⁸. These patterns were, in
124 some cases, also correlated with known tissue-specific functions or activities of these genes
125 (Supplementary Discussion 4).

126 Based on the skeletal phenotypes reported in previous studies analysing the effects of
127 decreased pH levels on corals^{12,19-21}, we initially expected that many of the differentially
128 methylated and differentially expressed genes would be involved in biomineralization.
129 However, among the calcification genes we characterized, relatively few genes responded.
130 Overall, we observed a minor shift in methylation of organic matrix (OM) and extracellular

131 matrix (ECM) components, with some known OM genes upmethylated and/or upregulated
132 and others downmethylated and/or downregulated, implying a possible change in the
133 scaffolding structure of the OM and ECM (Supplementary Discussion 5). As a general trend,
134 we observed that Ca^{2+} -binding OM constituents exhibited increased methylation and
135 expression, whereas genes involved in cell-cell adhesion exhibited decreased methylation and
136 expression.

137 Instead of biomineralization-related pathways, a functional enrichment analysis of
138 differentially methylated genes revealed processes linked to growth and stress response (Fig.
139 3a, Supplementary Data 3). More specifically, we observed that the methylation levels of
140 many genes in the MAPK signalling and cell growth pathways changed significantly (Fig.
141 3b). Remarkably, we found that the methylation levels of genes involved in the negative
142 regulation of JNK and MAPK increased; conversely, the methylation levels of genes that
143 positively regulate the same kinases decreased (Fig. 3c). For instance, the methylation of JIP1
144 (JNK-interacting protein 1, SpisGene10613), a negative regulator of JNK, increased in both
145 aboral and oral tissues at pH 7.2; while the methylation of TRAF6 (TNF receptor-associated
146 factor 6, SpisGene580), a positive regulator of JNK, decreased in both tissues. The JNK
147 pathway has previously been shown to control cell, organ and body size in response to stress
148 in mice²² and *Drosophila*²³. The consistent differential methylation of JNK effectors that we
149 observed in *S. pistillata* in response to decreasing pH levels therefore suggested a change in
150 cell and body size.

151



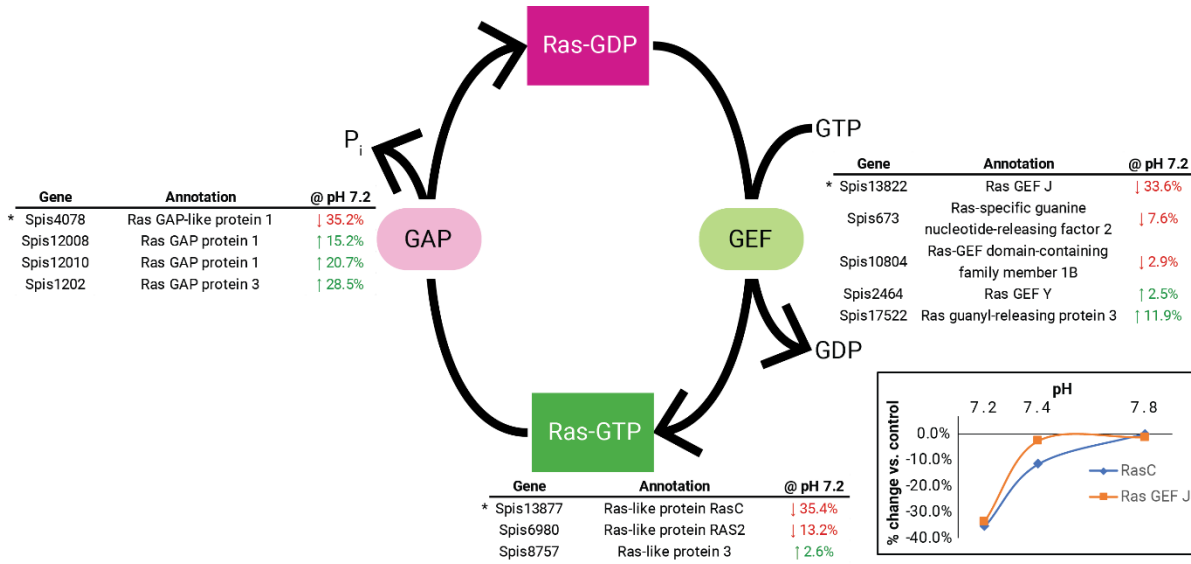
152

153 **Figure 3: Differential methylation of genes in the MAPK/JNK signalling and cell growth**
154 **pathways in the coral *S. pistillata* under pH stress.** (a) The majority of the growth- and
155 stress response-related GO terms are significantly enriched at pH 7.2. (b) At pH 7.2, more
156 genes respond with a significant increase (red) than with a decrease (blue) in methylation;
157 genes shaded in grey are methylated but not differentially regulated. (c) The methylation of
158 genes that negatively regulate MAP kinase and JUN kinase (red lines) increases, whereas the
159 methylation of genes that positively regulate the same kinases (blue lines) decreases in a
160 reciprocal manner (error bars denote ± 1 SE).

161

162 Analysis of differentially expressed genes in the MAPK and cell growth pathways
163 highlighted several key genes that are differentially expressed in a manner that suggests a
164 delay in cell division and an increase in cell size and body growth. For instance, Mos, a
165 kinase that has been shown to prevent the degradation of cyclin B and thereby delay the onset

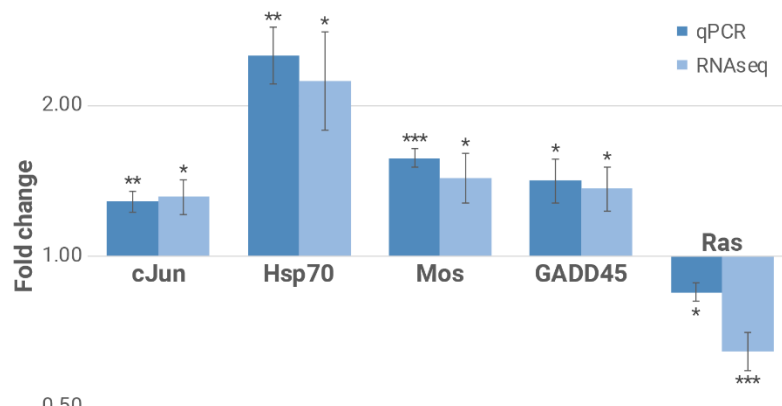
166 of the anaphase²⁴, was upregulated. Similarly, GADD45, a gene that binds to CDK1 and
167 prevents its association with cyclin B, was also upregulated, potentially delaying the onset of
168 M phase²⁵. In contrast, Ras, which plays a key role in the progression of the G1 phase, was
169 downregulated²⁶. The kinases and phosphatases that regulate Ras experienced concomitant
170 changes that indicated an overall reduction in Ras activity (Extended Data Fig. 1). For the
171 latter, we observed expression increases in c-JUN, a transcription factor that promotes
172 cellular growth; and Hsp70, previously observed in coral larvae under prolonged pH stress
173 and presumably expressed to assist in the correct folding of cellular proteins²⁷. The
174 differential expression of these genes was subsequently corroborated via a quantitative
175 reverse transcription PCR (RT-qPCR) analysis (Extended Data Fig. 2, Supplementary Data
176 4).



177
178 **Extended Data Figure 1: Downregulation of Ras and Ras guanine nucleotide-exchange**
179 **factors (GEFs) and upregulation of Ras GTPase-activating proteins (GAPs) suggest a**
180 **reduction in active Ras.** The molecular switch regulating the activation of Ras is dependent
181 on the activities of two opposing classes of proteins: GAPs, which convert the active Ras-
182 GTP to the inactive Ras-GDP form, and GEFs which convert Ras-GDP to Ras-GTP. At pH

183 7.2, the Ras homologues present in *S. pistillata* (Spis8757, Spis6980 and Spis13877) had
184 reduced expression. This occurred in tandem with the general upregulation of Ras GAPs and
185 downregulation of Ras GEFs, thus further depleting the amount of active Ras-GTP under pH
186 stress. Asterisks denote significant differential expression ($p < 0.05$). (inset) The significantly
187 downregulated Ras homologue (Spis13877, blue) and Ras GEF (Spis13822, orange)
188 exhibited differential expression exclusively at pH 7.2.

189



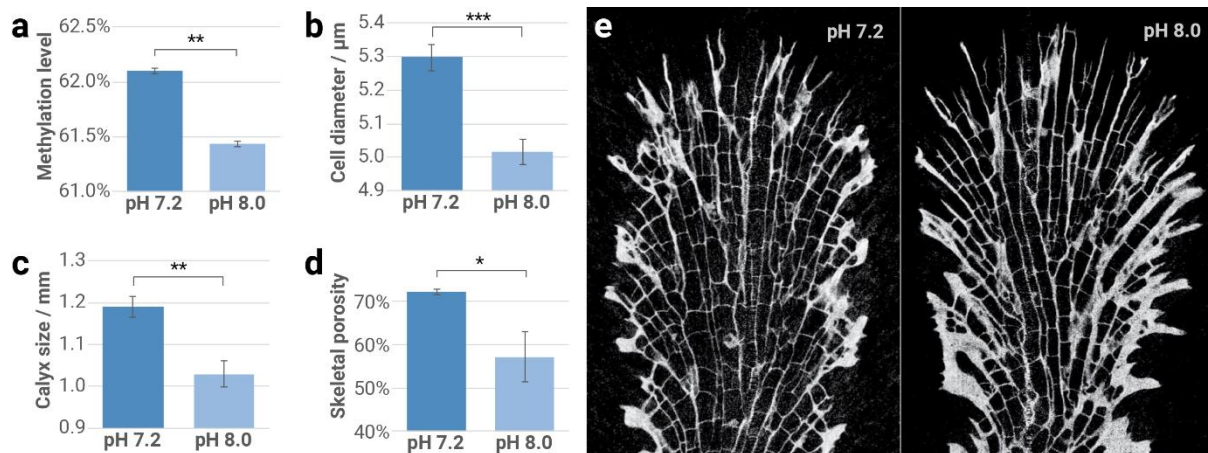
190

191 **Extended Data Figure 2: Differential expression of key genes was corroborated using**
192 **RT-qPCR.** Fold change indicates the expression of these genes at pH 7.2 relative to the
193 control (pH 8.0). The experimentally measured values are very similar to that of RNA-seq,
194 providing further support for the findings. Error bars represent ± 1 SE. Asterisks denote
195 significance of t -test p values. *: $p < 0.05$; **: $p < 0.01$; ***: $p < 0.001$.

196

197 In light of our data, we hypothesised that changes in DNA methylation (Fig. 4a) and
198 expression of key genes lead to an increase in cell size at pH 7.2. We first confirmed that
199 individual cell sizes were significantly larger in corals grown at pH 7.2 relative to the control
200 (total $n = 4,728$ measurements across 14 nubbins, Fig. 4b, Supplementary Data 5a). We then
201 hypothesized that this cell-level phenotypic change would be accompanied by a

202 corresponding increase in polyp size, and ultimately, skeletal structure. Specifically, we
203 posited that larger cells form larger polyps and larger corallite calyxes (the cup-shaped
204 openings in the skeleton that house the polyps). As measuring the size of polyps is difficult
205 due to their expandable/contractible nature, we opted to measure the size of the calyx as a
206 proxy. As predicted, our analyses confirmed that the calyxes in corals grown at pH 7.2
207 relative to the control were indeed significantly larger (total $n = 181$ measurements across 10
208 nubbins, Fig. 4c, Supplementary Data 5b). Finally, we also confirmed that the skeleton was
209 significantly more porous ($n = 6$ nubbins, Fig. 4d, e) in samples from the same treatment. All
210 of the observed phenotypes were consistent with our hypothesis.



211
212 **Figure 4: Effect of lower pH levels on cell growth.** (a) Mean methylation levels were
213 significantly increased at pH 7.2. (b) Cell sizes were significantly larger in nubbins grown in
214 the pH 7.2 tank. (c) Larger cell sizes translated to larger polyps and consequently to a skeletal
215 structure that contained larger calyxes. (d) The skeletal porosity was significantly higher at
216 lower pH. (e) Representative longitudinal sections of *S. pistillata* skeletons under pH 7.2 and
217 pH 8.0. Error bars represent 1 SE. Asterisks denote significance of *t*-test *p* values. *: *p* < 0.05;
218 **: *p* < 0.01; ***: *p* < 0.001.

219

220 It is important to note that while our results show a strong correlation between changes in

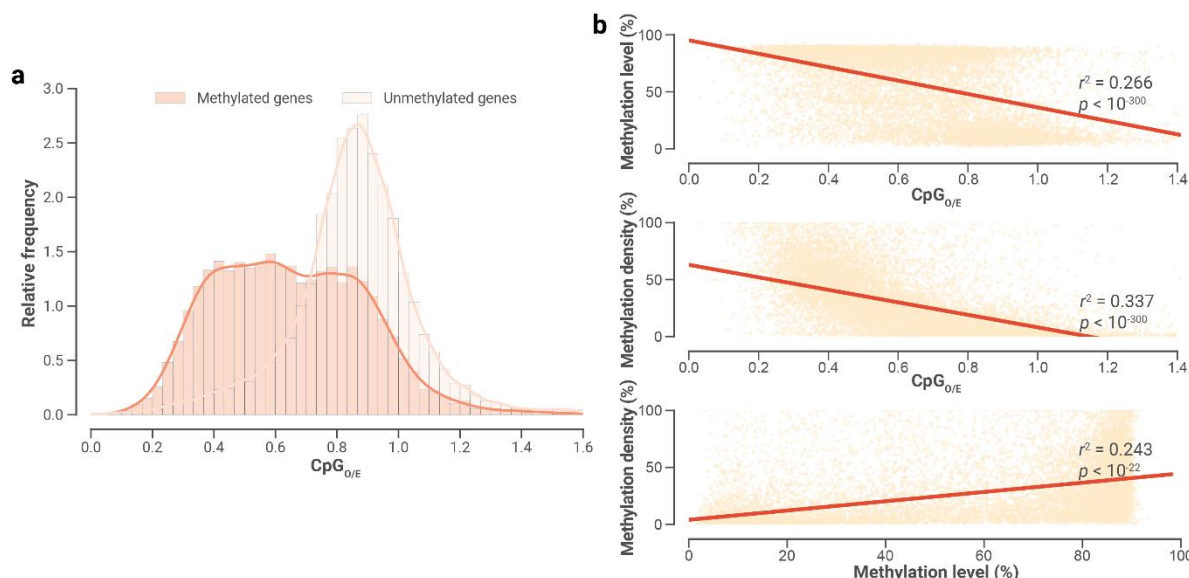
221 DNA methylation and the resulting phenotype, they do not show a *sensu stricto* causal
222 relationship between changes in the methylation state and the phenotype. However, the high
223 reproducibility of the changes in methylation and the presence of tissue-specific DNA
224 methylation patterns lend support for a function of DNA methylation in phenotypic plasticity.
225 Our results suggest that the observed phenotypic changes under pH stress are mediated
226 through differential methylation and expression of known stress response pathways that
227 control cell proliferation and growth^{22,23}. We propose that these cellular phenotypic changes,
228 together with shifts in organic matrix proteins, are among the drivers of morphological
229 changes in the skeleton of this species under seawater acidification observed here and
230 described previously¹². These morphological changes towards a more porous skeleton are
231 possibly a means by which *S. pistillata* can maintain linear extension rates in the face of
232 depressed calcification rates under seawater acidification^{12,28}. Such a trait would be
233 advantageous in the benthic environment where competition for space and light is an
234 important selective pressure²⁹.
235 In conclusion, our results suggest that DNA methylation could offer corals greater ability to
236 buffer the impacts of environmental changes and provide additional time for genetic
237 adaptation to occur. Better understanding of the mechanisms underlying coral resilience will
238 also provide additional avenues for reef-restoration efforts, such as the human-assisted
239 acclimatization of corals in specialised nurseries (“designer reefs”³⁰). Such efforts might
240 prove crucial to averting large-scale losses of extant coral reefs in light of recent global
241 declines due to climate change.
242

243 **Supplementary Discussion**

244 **SD1. Comparisons with previous methylation studies in corals**

245 In the absence of direct evidence, earlier work in corals^{7,8,10} based the identification of
246 methylated genes on two assumptions. Firstly, methylated genes have coding sequences with
247 fewer CpG dinucleotides than expected. This is usually quantified with CpG_{O/E} (also termed
248 “CpG bias”), which represents the ratio of observed versus expected CpG dinucleotides on a
249 per-gene basis. Secondly, strongly methylated genes have both high methylation levels (a
250 particular CpG is methylated in most cells) and high methylation density (most CpGs in that
251 gene are methylated).

252 Our data show that there are exceptions to both assumptions. A low CpG_{O/E} value (< 0.6) is
253 fairly indicative of methylated genes, but classifying genes above the same threshold as
254 unmethylated would include many genes that are methylated (Extended Data Fig. 3a). This
255 could be from genes acquiring methylation at different evolutionary times and/or the presence
256 of different selection pressures for methylated cytosines that undergo spontaneous
257 deamination. Also, while correlations between CpG_{O/E}, methylation level and methylation
258 density in the expected direction exist, the strengths of the correlations are moderate at best
259 (Extended Data Fig. 3b).



260

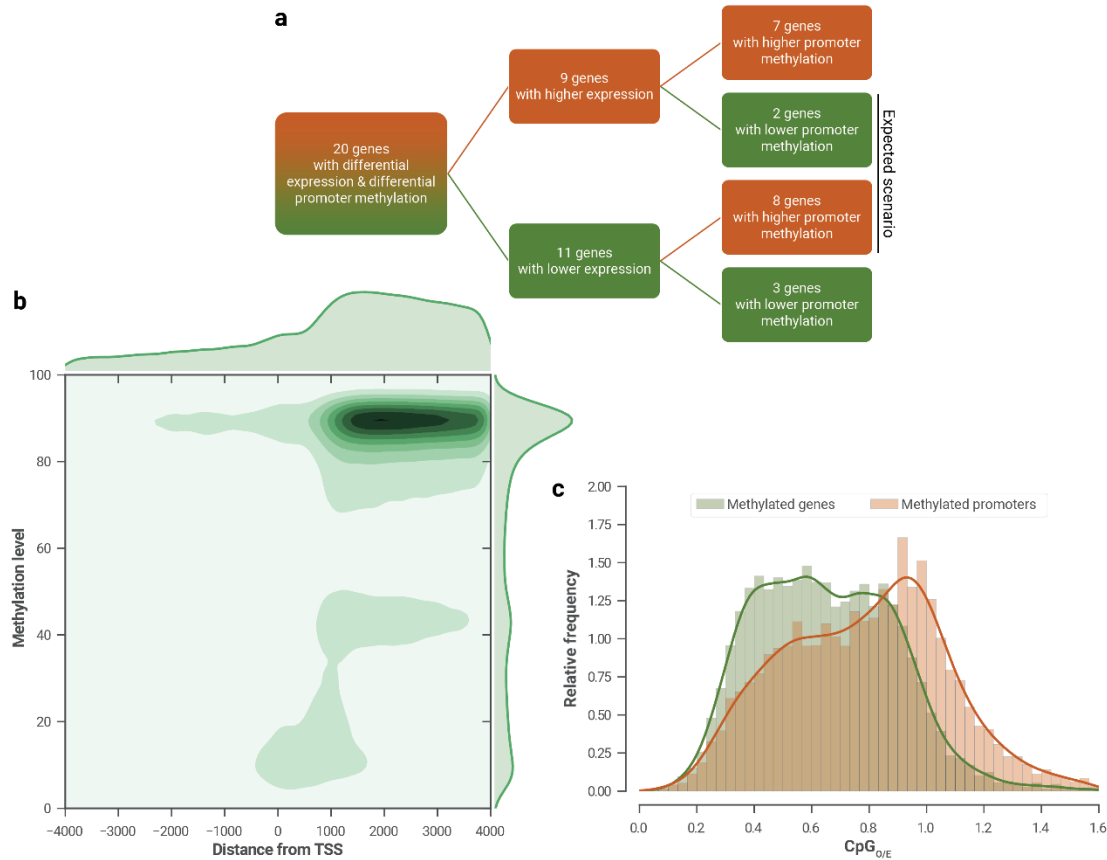
261 **Extended Data Figure 3: Distribution of CpGo/E (“CpG bias”) for genes in *S. pistillata*.**

262 (a) While methylated genes do tend to have lower CpGo/E values than non-methylated genes,
263 a sizable fraction of methylated genes will be falsely considered non-methylated if a strict
264 CpGo/E threshold is used to define methylation states of genes. (b) Both metrics show
265 moderate but statistically significant inverse correlation with CpGo/E. There is a moderately
266 positive correlation between methylation level and methylation.

267

268 **SD2. *S. pistillata* promoter methylation has no effect on gene expression**

269 Methylation in vertebrates has primarily been thought to drive gene expression via the
270 differential methylation of promoter regions³¹. Our analysis indicates that—unlike in
271 vertebrates—promoter methylation in *S. pistillata* is sparse and does not influence gene
272 expression. We detected methylation in promoters (defined as a 4 kb window upstream of
273 genes) of 6,675 genes (25.9% of all genes). We identified 720 expressed genes that had
274 differential promoter methylation. Of these genes, only 20 genes were differentially
275 expressed ($p = 0.26$, Fisher’s exact test), but only half of these genes exhibited the expected
276 change in expression linked to the change in promoter methylation (Extended Data Fig. 4a).
277 Also, methylated promoters are generally less methylated than are gene bodies, as evidenced
278 through direct sequencing (Extended Data Fig. 4b) and CpG bias (Extended Data Fig. 4c),
279 indicating that methylation was either established in gene bodies earlier in evolutionary time
280 than in promoter regions, or gene bodies consistently have had higher levels of methylation
281 than promoters have had.



282

283 **Extended Data Figure 4: Multiple lines of evidence suggesting that promoter**
284 **methylation does not influence expression patterns in *S. pistillata*.** In these figures,
285 promoter regions are defined as 4 kb windows upstream from the transcriptional start sites of
286 all gene models. (a) Decision tree of 20 genes with differential gene expression and
287 differential promoter methylation at pH 7.2 relative to the control. Only half of the genes
288 exhibited the expected transcriptional response (i.e., increased promoter methylation
289 represses expression and vice versa) (b) This heatmap of methylation levels in 4 kb windows
290 upstream and downstream of transcription start sites demonstrates that methylation in
291 promoter regions was much lower than that in gene bodies. (c) CpG_{0/E} values were much
292 lower in gene bodies than in promoters.

293

294 **SD3. Correlation of genic expression to methylation**

295 In light of the crosstalk between transcription, histone modifications and gene body
296 methylation, in which highly expressed genes are methylated to suppress spurious
297 transcription from cryptic promoters¹¹, we sought to investigate whether similar observations
298 apply to corals.

299 We first confirmed that expression of methylated genes is higher than unmethylated genes in
300 *S. pistillata* (Fig. 2a). For methylated genes, expression levels were significantly higher in
301 genes with higher methylation levels, and in genes with higher methylation density up to 40%
302 (Fig. 2b). We also observed that genes that are highly methylated tended to be housekeeping
303 genes (Supplementary Data 6b), in line with indirect evidence from three other corals from
304 genus *Acropora*^{7,8}.

305 To quantify the amount of spurious transcription, we calculated the expression of the first few
306 exons relative to the first exon, with the expectation that methylation would reduce the
307 expression of the middle exons. Our RNA-seq data showed that, for methylated genes, there
308 was a progressive reduction of internal expression across the genes, culminating in a
309 significant difference observed in exon 6. The decline was also more significant when we
310 restricted the analysis to highly methylated genes (Fig. 2c).

311 Some reports have suggested a link between increased methylation and the reduction in
312 transcriptional variability (i.e., transcriptional noise)^{7,17}, estimated as the coefficient of
313 variation among the measured gene expression values. As previous studies did not investigate
314 whether expression values could be a confounding factor for transcriptional noise, we sought
315 to model transcriptional noise as a function of both expression level and methylation state.
316 Our GLM analysis indicates that while expression level largely (73.4–74.3%, $p < 0.0001$)
317 determines transcriptional noise, the presence of methylation in a gene further reduces (25.7–

318 26.6%, $p < 0.001$) the noise, consistent with a suppressive action of methylation on
319 expression (Extended Data Table 1).

320

321 **Extended Data Table 1: Modelling transcriptional noise as a function of expression level**
322 **and methylation state.** In our GLM analysis, the inverse of the coefficient of variation (cv^{-1})
323 was correlated against methylation status (0 for unmethylated genes; 1 for methylated genes)
324 and \log_{10} -transformed expression values. Among the tested variables, expression had the
325 greatest determinant of transcriptional noise (11.74), followed by an expression-dependent
326 coefficient that is present only in methylated genes (4.44). Methylation state, on its own, has
327 close to negligible effect on transcriptional noise (-0.19). All variables significantly influence
328 transcriptional noise ($p < 0.001$).

Model family: gamma
Link function: identity
Dependent variable: cv^{-1}
No. observations: 22,211
df model: 3
df residuals: 22,207

					95% confidence interval	
	Coefficient	Standard error	z	P> z	[0.025	0.975]
Intercept	1.006	0.0349	28.8416	0.0000	0.9376	1.0743
expression	11.7377	0.089	131.8157	0.0000	11.5632	11.9122
methylation_state	-0.1942	0.0553	-3.5079	0.0005	-0.3026	-0.0857
expression:methylation_state	4.4417	0.1253	35.4583	0.0000	4.1962	4.6872

329

330

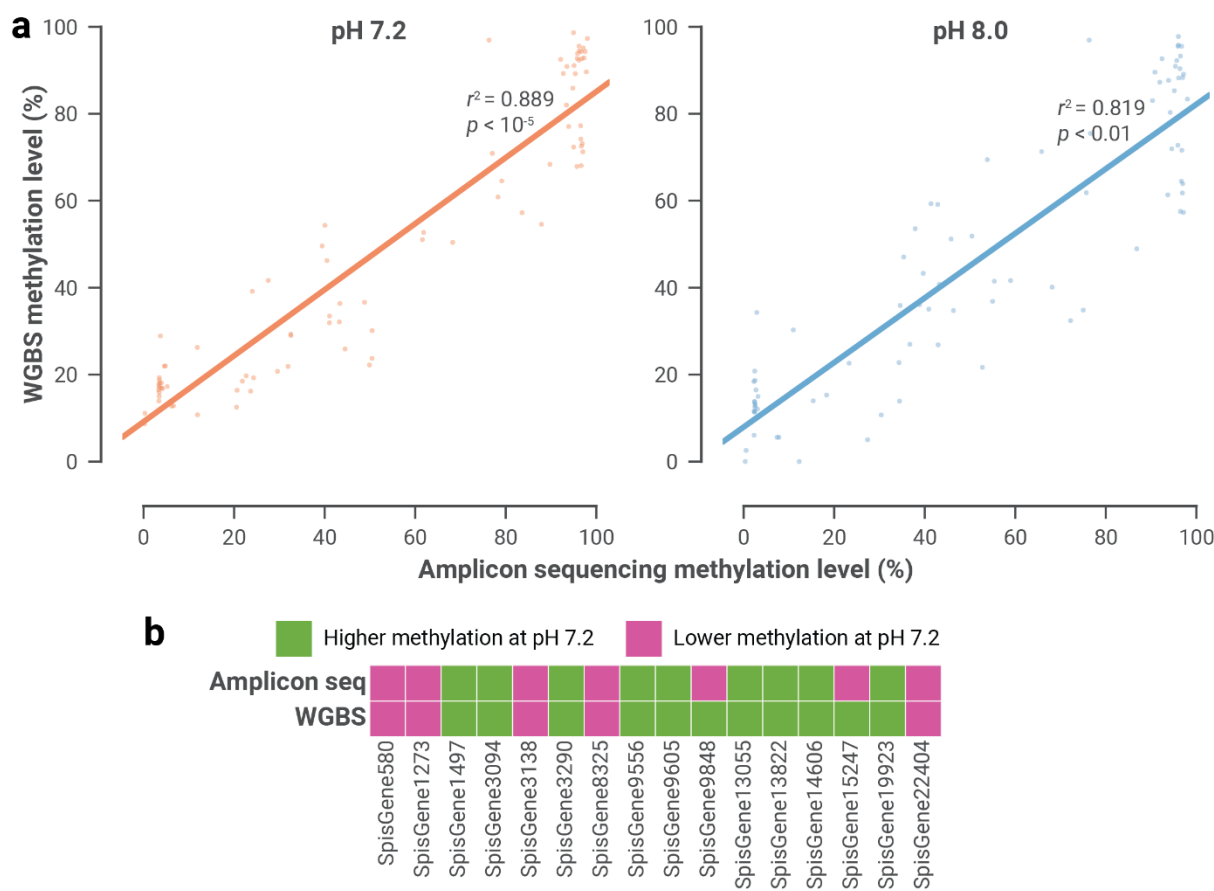
331 **SD4. Validation of methylation patterns**

332 To validate our initial findings and their reproducibility, we used MiSeq-based amplicon-
333 specific bisulphite sequencing of selected candidate genes on the original samples as well as
334 on samples from an independent repeat experiment.

335 Accuracy of amplicon-specific bisulphite sequencing was assessed by performing this

336 technique on DNA from all three biological replicates from the pH 7.2 and control treatments
337 that were used to construct the original whole genome bisulphite libraries. Methylation levels
338 of individual CpGs assayed using both techniques were highly correlated ($r^2 > 0.8$, $p < 0.01$,
339 Extended Data Fig. 5a, Supplementary Data 7). For most of the designed amplicons, both
340 techniques produced concordant predictions of the shift in methylation state at pH 7.2
341 (binomial test $p(X \geq 14) = 0.002$, Extended Data Fig. 5b).

342



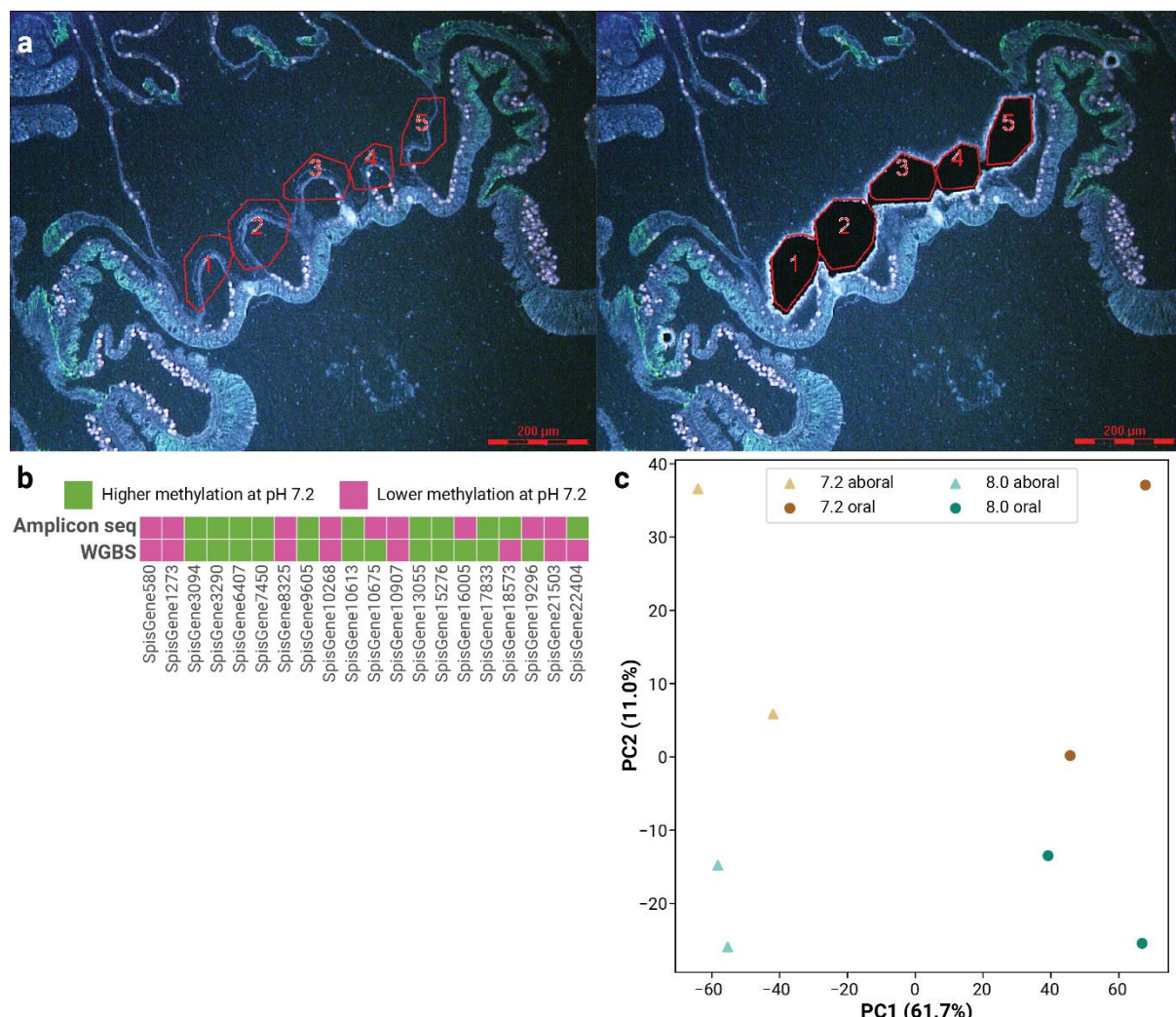
343

344 **Extended Data Figure 5: Amplicon-specific bisulphite sequencing can accurately assay**
345 **methylation levels of amplicons of interest.** (a) Results from amplicon sequencing largely
346 corroborated that from whole genome bisulphite sequencing ($r^2 > 0.8$ and $n = 3$ per
347 treatment). (b) It also produced the expected methylation pattern in most of the tested
348 amplicons (14 of 16 genes, binomial test $p(X \geq 14) = 0.002$).

349

350 To verify that the observed methylation changes are also reproducible, and at the same time
351 investigate whether methylation changes exhibited tissue-specific patterns, we performed
352 laser microdissections on samples from an independent experiment with the same conditions
353 as the previous pH 7.2 and 8.0 samples. We separated the aboral tissues from the oral tissues
354 (Extended Data Fig. 6a), and subsequently carried out amplicon-specific bisulphite
355 sequencing on the extracted DNA. Of the 20 genes tested, amplicon sequencing confirms that
356 15 genes were differentially methylated in the expected direction (Extended Data Fig. 6b,
357 Supplementary Data 8, binomial test $p(X \geq 15) = 0.02$).

358



359

360 **Extended Data Figure 6: Methylation patterns are strongly tissue-specific.** (a) Example
361 laser microdissection of aboral tissue from a fixed sample (scale bar represents 200 μ m). (b)
362 15 out of 20 genes (binomial test $p(X \geq 15) = 0.02$) showed the expected methylation patterns
363 (i.e., loci that had higher/lower methylation at pH 7.2) in samples from a separate experiment.
364 (c) PCA on these loci show that methylation patterns have a very strong tissue-specific
365 signature (along PC1); less so by treatment (along PC2).

366

367 Interestingly, we find that tissue-specific methylation patterns are stronger than treatment-
368 specific patterns (Extended Data Fig. 6c). This observation ties in well with studies done on
369 humans¹⁸, where non-cancerous cell lines tended to cluster based on tissue of origin.

370 Nonetheless, the effect of the long-term pH stress is evident: the second principal component
371 of the Principal Component Analysis (PCA) cleanly separates the treatments from each other.

372 Among the tested amplicons, some had similar methylation levels in both tissues, while stark
373 differences were present in some others. For example, major yolk protein (Spis7450), which
374 is found in the skeletal organic matrix, has a mean methylation level of 26.2% in aboral
375 tissues, in contrast to the 8.5% in oral tissues. Catalase (SpisGene3094), which has previously
376 been associated with symbiosis, has a 13.6% methylation in aboral tissues, a third of the
377 43.3% in the oral tissues where most of the symbionts reside.

378 Unexpectedly, genes that are involved in the regulation of JNK also displayed tissue-
379 specificity. TRAF6 (SpisGene580) and JNK-interacting protein 1 (SpisGene10613) were far
380 more methylated in oral tissues than aboral. This potentially indicates that these genes might
381 be regulated in a tissue-specific manner.

382

383 **SD5. Differential expression and methylation of biomineralization genes**

384 pH stress has been consistently linked to the differential regulation of biomineralization genes
385 in scleractinian corals³²⁻³⁴; however, its effect on methylation patterns has yet to be studied.
386 Our analysis of differentially methylated and differentially expressed biomineralization genes
387 did not correlate well with the observed phenotype. Also, the corresponding methylation
388 landscape of these genes was strikingly different from that of expression (Extended Data Fig.
389 7, Supplementary Data 9). This indicates that pathways responding to pH stress are perhaps
390 under direct expression regulation via transcriptional factors, rather than affected by the fine-
391 tuning of expression afforded via changes in methylation state.



395 0.05) in one or more experimental conditions. Genes are sorted by the mean increase in
396 expression, followed by the mean increase in methylation. Grey boxes represent changes in
397 expression or methylation that were not statistically significant; blank boxes represent
398 unmethylated genes. The heatmaps show little overlap between differentially expressed genes
399 and differentially methylated ones, but the expression and methylation responses were always
400 more pronounced at lower pH.

401

402 Among the differentially methylated genes, we identified two genes encoding key ion
403 transporters putatively involved in the calcification process. The first is a gene encoding the
404 carbonic anhydrase STPCA (Spis16865) that has previously been localized in the ECM and is
405 thought to facilitate calcification by hydrating local CO₂ to HCO₃⁻³². The gene for this
406 protein was more methylated in the pH 7.2 and 7.4 treatments, indicating a potential
407 compensating mechanism that increases HCO₃⁻ concentration. The second gene encodes the
408 bicarbonate transporter SLC4β (Spis8325), which is thought to be coupled to the enzyme
409 STPCA2 in calicoblastic cells to facilitate HCO₃⁻ transport to the ECM³⁵. This gene,
410 however, is less methylated at pH 7.2, potentially indicating a modulation of bicarbonate ion
411 transport to the ECM.

412 Interestingly, we also observed increased expression of CARP1 (Spis6759), a main
413 constituent of the OM. This gene has been shown to be important for mineral deposition³⁶
414 and is localized in the cells around the skeleton³⁷. CARPs and analogous proteins can bind to
415 collagen—the former serving as mineral nucleation points, while the latter providing
416 structural support within the ECM. An increase in CARP transcription may indicate an
417 increase in possible nucleation points for growth of the coral skeleton and might represent a
418 compensation mechanism. Major yolk protein (MYP, Spis7450), another OM protein with

419 elevated expression³⁶, is unusual in also having increased methylation at pH 7.2. MYP binds
420 and shuttles ferric iron³⁸, which is an important trace element in the coral skeleton and
421 potentially plays a photoprotective role³⁹. Furthermore, we found a putative homologue of
422 bone morphogenetic protein (BMP1, Spis8057) that was upregulated at pH 7.2. This protein
423 was also found to be highly expressed in embryos of the sea urchin *Strongylocentrotus*
424 *purpuratus* immediately before primitive skeleton (spicule) formation⁴⁰, possibly indicating a
425 positive role in calcification.

426

427 **Methods**

428 **Growth conditions of *S. pistillata***

429 Colonies of the tropical coral *Stylophora pistillata* were exposed to long-term seawater
430 acidification as described previously^{12,13}. Briefly, corals were kept *in aquaria* supplied with
431 Mediterranean seawater (exchange rate of 70% h⁻¹) at a salinity of 38 g L⁻¹, temperature of
432 25 °C and irradiance of 170 mmol photons m⁻² s⁻¹ on a 12h/12h photoperiod provided by
433 HQI-10000K metal halide lamps (BLV Nepturion, Steinhoering, Germany). Carbonate
434 chemistry was manipulated by bubbling CO₂ to reduce the control pH (pH 8.0) to the target
435 values of pH 7.8, 7.4, and 7.2. Values of carbonate chemistry parameters were as previously
436 measured: 3792, 2257, 856 and 538 µatm respectively for pH 7.2, 7.4, 7.8 and 8.0¹².

437 **Identification of methylated CpGs**

438 DNA was extracted from *S. pistillata* nubbins (triplicates of four growth conditions) using a
439 nuclei isolation approach to minimize contamination with symbiont DNA, as previously
440 described (Voolstra et al., 2017, in review). Briefly, cells from *S. pistillata* from a nubbin of
441 about 3 cm were harvested using a Water Pick in 50 ml of 0.2 M EDTA solution refrigerated
442 at 4 °C. Extracts were successively passed through a 100 µm and a 40 µm cell strainer

443 (Falcon, Corning, NY) to eliminate most of the algal symbionts. Extracts were then
444 centrifuged at 2,000g for 10 min at 4 °C. The supernatant was discarded and the resulting
445 pellets were homogenized in lysis buffer (G2) of the Qiagen Genomic DNA Isolation Kit
446 (Qiagen, Hilden, Germany). The DNA was extracted following manufacturer instructions
447 using Genomic-tip 100/G (Qiagen, Hilden, Germany). DNA concentration was determined
448 by O.D. with Epoch Microplate Spectrophotometer (BioTek, Winooski, VT). Contamination
449 with *Symbiodinium* DNA was assessed via PCR targeting the multicopy gene RuBisCO
450 (Genbank accession number AY996050).

451 Bisulphite DNA libraries were prepared following a modified version of the NEBNext Ultra
452 II DNA Library Prep Kit for Illumina (NEB, Ipswich, MA). Methylated TruSeq Illumina
453 adapters (Illumina, San Diego, CA) were used during the adapter ligation step followed by
454 bisulphite conversion with the EpiTect Bisulfite kit (Qiagen, Hilden, Germany), with the
455 following cycling conditions (95 °C for 5 min, 60 °C for 25 min, 95 °C for 5 min, 60 °C for
456 85 min, 95 °C for 5 min, 60 °C for 175 min, then 3 cycles of 95 °C for 5 min and 60 °C for
457 180 min. Hold at 20 °C ≤ 5 hours). The final library was enriched with the KAPA HiFi
458 HotStart Uracil+ ReadyMix (2X) (KAPA Biosystems, Wilmington, MA) following the
459 standard protocol for bisulfite-converted NGS library amplification. Final libraries were
460 quality checked using the Bioanalyzer DNA 1K chip (Agilent, Santa Clara, CA), and
461 quantified using Qubit 2.0 (Thermo Fisher Scientific, Waltham, MA), then pooled in
462 equimolar ratios and sequenced on the HiSeq2000 platform. Sequencing of the libraries
463 resulted in 1.53 billion read pairs across 12 samples (Supplementary Data 1). The raw
464 sequences were trimmed using cutadapt v1.8⁴¹. Trimmed reads were then mapped to the *S.*
465 *pistillata* genome, deduplicated and scored on a per-position basis for methylated and
466 unmethylated reads using Bismark v0.13⁴².

467 To ensure that methylated positions were *bona fide*, three stringent filters were used. Firstly,

468 the probability of methylated positions arising from chance on a per-position basis was
469 modelled using a binomial distribution $B(n, p)$, where n represents the coverage (methylated
470 + unmethylated reads) and p the probability of sequencing error (set to 0.01 to mimic a Phred
471 score of 20). We kept positions with k methylated reads if $p(X \geq k) < 0.05$ (post-FDR
472 correction). Secondly, methylated positions had to have at least a methylated read in all three
473 biological replicates of at least one growth condition. Finally, the median coverage of the
474 position across all 12 samples had to be ≥ 10 . These steps ensured that methylated positions
475 were highly replicable and highly covered.

476 **Assignment of genomic context to methylated cytosines**

477 Based on the genome annotation of *S. pistillata* (in the form of a GFF3 file) and the positional
478 coordinates of the methylated cytosines (in a tab-separated file produced by Bismark), a
479 Python script was written to annotate every methylated cytosine with additional genomic
480 context. The script determined whether the methylated position resides in a genic or
481 intergenic region: for the former, an additional check occurs to determine whether it is in an
482 exon or an intron. Subsequently, distances to the 5' and 3' end of each genomic feature
483 (gene/intergenic region/exon/intron) were calculated.

484 **Identification of differentially methylated genes**

485 Using the methylation level of genes at pH 8.0 as a control, GLMs were implemented in R to
486 identify genes that were differently methylated at pH 7.2, 7.4 and 7.8 respectively. The
487 general formula used was:

488 `glm(methylated, non_methylated ~ pH * position, family="binomial")`

489 where “methylated, non_methylated” was a two-column response variable denoting the
490 number of methylated and non-methylated reads at a particular position, while “pH” and
491 “position” were predictor variables for the pH of the environment and the genomic coordinate

492 of the position respectively. Data from individual replicates were entered separately—this
493 approach assigned equal weightage to each replicate, instead of having a disproportionate
494 skew towards the replicate with the highest coverage if the data were pooled. Genes with < 5
495 methylated positions were filtered out to reduce type I errors.

496 **Identification of differentially methylated promoters**

497 As promoter regions were not defined in the *S. pistillata* genomes, it was assumed to be
498 located in a window of 4 kb upstream of the transcription start site. A GLM similar to the one
499 described in the previous paragraph was used to identify differentially methylated promoters;
500 however, due to the scarcity of methylated positions in these windows, genes with ≥ 2
501 methylated positions were retained for this analysis.

502 **Identification of differentially expressed genes**

503 High quality total RNA was extracted for library creation from 3 *S. pistillata* nubbins per
504 treatment. Directional mRNA libraries were produced using the NEBNext Ultra Directional
505 RNA Library Prep Kit for Illumina (NEB) as described in (Voolstra et al., 2017, in review).
506 A total of 674 million paired-end reads (read length of 101 bp) were retrieved from 6 lanes on
507 the HiSeq2000 platform (Illumina, San Diego, CA).

508 Trimming was intentionally left out to increase the number of mapped reads, and to reduce
509 bias⁴³. The resulting 362 million trimmed reads were mapped to *S. pistillata* gene models
510 with kallisto v0.42.4⁴⁴ to produce TPM (transcripts per million reads) values. Based on these
511 values, sleuth⁴⁵ was used to identify differentially expressed genes by contrasting all
512 biological replicates of pH 7.2, 7.4 and 7.8 against the controls (pH 8.0).

513 **Calculation of exon expression relative to first exon**

514 As kallisto is a pseudo-mapper, i.e., it assigns reads to gene models, but not the exact location
515 of where the read maps to the gene model, reads from all 12 replicates were mapped

516 separately using HISAT2 (v2.1.0)⁴⁶ against the *S. pistillata* genome. Genomic positions that
517 correspond to exonic locations were extracted with a Perl script, and mean coverages were
518 computed to produce RPKM values on a per-replicate, per-exon basis with a Python script.

519 Genes with six or more exons were selected for the analysis. Furthermore, as ratio-based
520 computations are skewed by lowly expressed genes, genes with overall mean RPKM > 0.5
521 and non-zero expression in the first six exons across all 12 replicates were selected. Ratios
522 were subsequently natural log-transformed to improve normality, resulting in 1,141
523 unmethylated genes, 5,750 methylated genes, and 2,955 highly methylated genes (genes with
524 median methylation > 80%).

525 **Functional enrichment of methylated genes**

526 GO term annotations were obtained from literature (Voolstra et al., 2017, in review). GO
527 term enrichment analyses were carried out with topGO⁴⁷ with default settings. GO terms with
528 $p < 0.05$ and occurring ≥ 5 times in the background set were considered significant. Multiple
529 testing correction was not applied on the resulting p -values as the tests were considered to be
530 non-independent⁴⁷.

531 KEGG Orthology (KO) annotations were merged from results of gene model annotation and
532 KAAS (KEGG Automatic Annotation Server), <http://www.genome.jp/tools/kaas/>, with
533 parameters “GHOSTZ”, “eukaryotes”, and “bi-directional best hit”. Based on the KO
534 annotation, KEGG pathway enrichment was carried out using Fisher’s exact test. Pathways
535 with $p < 0.05$ were considered significant.

536 **RT-qPCR verification of key growth genes**

537 There is only one reference amplicon (against β -actin) designed specifically for this
538 organism³². As normalization against a single reference gene is rarely acceptable⁴⁸, additional
539 control genes were selected from our RNA-seq data. Selected genes were highly abundant

540 (TPMs > 1,000), and expressed at roughly equivalent levels in all sequenced libraries.

541 Primers were designed, whenever possible, to include a large intronic region in addition to an
542 exonic size of ~100 bp. A Python script that interfaced with Primer3 v2.3.6⁴⁹ was written to
543 optimise primers design, e.g., melting temperatures of ~60 °C, GC% of 30–70%, avoid long
544 runs of a single base and no strong secondary structure.

545 A preliminary RT-PCR was run to confirm that amplicons produced band sizes
546 corresponding to the amplified exonic region; as expected, none of the primers produced
547 detectable bands that included the intronic regions. Six reverse transcription reactions (on
548 total RNA from all pH 7.2 and 8.0 replicates) were carried out with SuperScript III First-
549 Strand Synthesis SuperMix (Invitrogen, Carlsbad, CA) with the supplied oligo-dT primers.
550 The subsequent qPCR was carried out using Platinum SYBR Green qPCR SuperMix-UDG
551 (Invitrogen, Carlsbad, CA) in a 7900HT Fast Real-Time PCR System (Applied Biosystems,
552 Waltham, MA). Both protocols were carried out according to manufacturer's instruction.

553 Primer sequences, amplicon sizes, and the analysis of the RT-qPCR results are fully detailed
554 in Supplementary Data 4.

555 **Laser microdissection of *S. pistillata* samples**

556 Apexes of colonies were prepared as described previously⁵⁰. Briefly, apexes of *S. pistillata*
557 from an independent experiment using the same treatment conditions were fixed in 3%
558 paraformaldehyde in S22 buffer (450 mM NaCl, 10 mM KCl, 58 mM MgCl₂, 10 mM CaCl₂,
559 100 mM Hepes, pH 7.8) at 4 °C overnight and then decalcified, using 0.5 M
560 ethylenediaminetetraacetic acid (EDTA) in Ca²⁺-free S22 at 4 °C. They were then dehydrated
561 in an ethanol series and embedded in Paraplast. Cross-sections (6 µm thick) were cut and
562 mounted on POL-membrane (0.9 µm) frame slides (Leica Microsystems, Wetzlar, Germany).
563 The Leica AS LMD system, with a pulsed 337 nm ultraviolet laser on an upright microscope,

564 was used for the microdissections. The laser beam can be moved with a software-controlled
565 mirror system that allows selecting target cells and tissues. Target cells can be preselected on
566 a monitor with a freehand drawing tool, and then the computer-controlled mirror moves the
567 laser beam along the pre-selected path and the target cells are excised from the section. The
568 dissected part then falls into a PCR tube under gravity. The collection by gravity ensures
569 quick and contamination-free processing of the dissected tissue sections.

570 DNA from eight sections (duplicates of aboral and oral tissue from pH 7.2 and from controls)
571 were extracted, and subjected to bisulphite conversion using EpiTect Plus Bisulfite
572 Conversion kit following manufacturer's instructions (Qiagen, Hilden, Germany).

573 **Validation of differential methylation via amplicon-specific bisulphite sequencing**

574 As dissected tissues contain minute amounts of DNA, we decided to perform amplicon-
575 specific bisulphite sequencing to validate the methylation levels within our amplicons of
576 interest. A nested PCR design was used to generate these amplicons. Outer primers were
577 pooled in the initial PCR run (35 cycles), and the resulting reaction mix was then evenly split
578 into amplicon-specific individual PCR reactions (35 cycles) with their respective inner
579 primers. As the amplicons were to be sequenced on the Illumina MiSeq platform, the inner
580 primer pairs were designed with additional overhangs to facilitate downstream library
581 creation, per the 16S Metagenomic Sequencing Library Preparation guide (Illumina, San
582 Diego, CA).

583 Amplicons were selected within genes that exhibited differential methylation at pH 7.2
584 relative to control. As bisulphite-conversion produces Watson and Crick strands that are no
585 longer reverse complements of each other, primers were designed to amplify the sense strand
586 of the gene product. To optimise primer design, a self-written Python script that interfaced
587 with Primer3 v2.3.6⁴⁹ was used to select primer pairs that were fully located within non-

588 methylated regions. This important consideration avoids the need for degenerate primers (one
589 degenerate base is required per methylated CpG), reducing ordering costs and dodging
590 potential PCR amplification biases. In total, 46 amplicons (i.e., 184 primers) were designed.

591 To assess the primers, test nested PCRs were performed on converted *S. pistillata* total DNA;
592 PCR products were subsequently visualized on an agarose gel. Primers that completely failed
593 to produce amplicons with expected band sizes were discarded ($n = 3$). The remaining
594 primers were grouped into 3 batches (of ~14 primers each) to reduce unintended products that
595 might arise from pooling too many outer primers in the initial reaction.

596 To validate our original findings and to test the accuracy of this approach, the same
597 amplicon-specific bisulphite approach was carried out on DNA from all three samples of pH
598 7.2 and control that were used to construct the original whole genome bisulphite libraries.
599 This allowed for direct comparisons of methylation levels assayed via amplicon-specific and
600 whole genome bisulphite sequencing.

601 With the use of Nextera XT indices (Illumina, San Diego, CA), libraries were pooled and
602 sequenced on one-and-a-half MiSeq runs. A total of 14.2 million paired-end reads (read
603 length of 300 bp) were produced. These reads were cleaned and mapped to the *S. pistillata*
604 genome with the same pipeline used to process reads from whole genome bisulphite
605 sequencing, with the sole exception of skipping the deduplication step (distinct amplicons
606 from the same loci map to the same genomic coordinates and thus are erroneously deemed
607 duplicates).

608 We used a very conservative coverage threshold for the downstream analyses: only
609 methylated positions with read coverages greater than 100 in all samples were retained. This
610 filtering step increased the precision of the measured methylation levels and reduced the
611 effect of noise on the results.

612 **Measurement of cell sizes**

613 As described previously²⁸, branches of 2–3 cm size were sampled from colonies grown in pH
614 7.2 and 8.0 treatment and placed in a 7% MgCl₂ solution to anesthetize tissues. Oral discs
615 (the apparent portion of the polyp) were then cut from the colony under a microscope using
616 microdissection scissors with 5 mm blades. Cells were then dissociated using a sterile tube
617 pestle and homogenized by repeated pipetting using a 200 µl pipette. Suspended cells (50 µl)
618 were mounted between the slide and coverslip, and 30 random pictures of the surface were
619 taken. Cell sizes on these pictures were subsequently measured using SAISAM software
620 (Microvision Instruments, France). In all, 4,728 measurements were taken across 14 tested
621 nubbins (Supplementary Data 5a).

622 **Measurement of corallite calyx size**

623 Branches of similar size (2 cm in length) were sampled from colonies in the pH 7.2 and 8.0
624 treatments and placed in a 10% NaClO solution for 2 h to remove tissues. Skeletons were
625 rinsed several times in tap water, followed by ultra-pure H₂O, and then dried at 40 °C for at
626 least 24 h. Samples (5 replicates per pH condition) were coated with gold/palladium and
627 observed at 4 kV with a JEOL 6010LV electron microscope. Diameters of the corallite
628 calyxes were measured using manufacturer-provided SMile View software (JEOL, Tokyo,
629 Japan). A total of 181 measurements were performed across 10 branches (Supplementary
630 Data 5b).

631 **Measurement of skeletal porosity**

632 The non-invasive, high-resolution imaging method of X-ray micro-computed tomography
633 (micro-CT) was used as described to measure skeletal porosity¹². Micro-CT analysis was
634 carried out at the Polyclinique St Jean, Cagnes sur Mer, France, with an SkyScan 1173
635 compact micro-CT (SkyScan, Antwerp, Belgium). A microfocus X-ray tube with a focal spot
636 of 10 mm was used as a source (80 kV, 100 µA). The sample was rotated 360° between the

637 X-ray source and the camera. Rotation steps of 1.5° were used. At each angle, an X-ray
638 exposure was recorded on the distortion-free flat-panel sensor (resolution 2,240 × 2,240
639 pixels). The resulting slice was made of voxels, the three-dimensional equivalent of pixels.
640 Each voxel was assigned a grey value derived from a linear attenuation coefficient that relates
641 to the density of materials being scanned. All specimens were scanned at the same voxel size.
642 The radial projections were reconstructed into a three-dimensional matrix of isotropic voxels
643 ranging from 5 to 10 mm, depending on the exact height of the coral tip. X-ray images were
644 transformed by NRecon software (SkyScan) to reconstruct two-dimensional images for
645 quantitative analysis. From these images, evaluation of the morphometric parameters was
646 performed using CT-Analyser software (SkyScan). A manual greyscale threshold was
647 implemented manually on the first set of images and then applied to all specimens. For each
648 sample, a digital region of interest was created to extend through 100 µm of skeleton at 7 mm
649 distance from the apex, corresponding to about 15 slices. The percentage of negative space in
650 relation to the skeleton was then determined, providing the measure of porosity. For each
651 treatment condition, three branches of similar size were taken from the apical part of a
652 colony. Porosity was analysed in one experimental trial with three replicates per treatment.

653

654 **Accession codes**

655 **Whole genome bisulphite sequencing and transcriptomic data**

656 PRJNA386774.

657

658 **Acknowledgements**

659 We thank Dominique Desgre, Natacha Caminiti-Segonds and Nathalie Techer for assistance
660 in coral husbandry; the KAUST Sequencing Core Facility for the sequencing of the libraries;

661 Nathalie Techer for cell size measurements; and Pierre Alemanno and Christophe Sattonnet
662 (Polyclinique St Jean, Cagnes sur Mer, France) for access to the micro-CT. This publication
663 is based upon work supported by the King Abdullah University of Science and Technology
664 (KAUST) Office of Sponsored Research (OSR) under Award No. FCC/1/1973-22-01.

665

666 **Author information**

667 **Affiliations**

668 **Red Sea Research Center, King Abdullah University of Science and Technology, Saudi
669 Arabia**

670 Yi Jin Liew, Yong Li, Craig T. Michell, Guoxin Cui, Christian R. Voolstra & Manuel Aranda

671 **Centre Scientifique de Monaco, Marine Biology Department, Principality of Monaco**

672 Didier Zoccola, Eric Tambutté, Sylvie Tambutté, Denis Allemand & Alexander A. Venn

673 **Computational Science Lab, Faculty of Science, University of Amsterdam, Amsterdam,
674 The Netherlands**

675 Eva S. Deutekom & Jaap A. Kaandorp

676 **Passed away 17 December 2016**

677 Sylvain Forêt

678 **Contributions**

679 M.A. conceived and coordinated the project. M.A., C.R.V., D.Z., E.T., S.T., D.A. and A.A.V
680 provided tools, reagents and/or data. C.T.M. constructed libraries for whole genome
681 bisulphite sequencing and RNA-seq. Y.J.L., Y.L., E.S.D., J.A.K. and M.A. analysed
682 expression data. Y.J.L., S.F. and M.A. analysed methylation data. Y.J.L., D.Z., G.C. and M.A.

683 performed tissue-specific experiments. E.T. and A.A.V. performed and analysed skeleton
684 parameters measurements. Y.J.L. and M.A. wrote the manuscript. All authors except for S.F.
685 (passed away) read and approved the final manuscript.

686 Competing financial interests

687 The authors declare no competing financial interests.

688 Corresponding author

689 Correspondence to: Manuel Aranda.

690 References

- 691 1. Hoegh-Guldberg, O. *et al.* Coral reefs under rapid climate change and ocean
692 acidification. *Science* **318**, 1737-1742 (2007).
- 693 2. Hughes, T. P. *et al.* Global warming and recurrent mass bleaching of corals. *Nature*
694 **543**, 373-377 (2017).
- 695 3. Frieler, K. *et al.* Limiting global warming to 2 °C is unlikely to save most coral reefs.
696 *Nat. Clim. Change* **3**, 165-170 (2013).
- 697 4. van Oppen, M. J., Oliver, J. K., Putnam, H. M. & Gates, R. D. Building coral reef
698 resilience through assisted evolution. *Proc. Natl. Acad. Sci. U S A* **112**, 2307-2313
699 (2015).
- 700 5. Feil, R. & Fraga, M. F. Epigenetics and the environment: emerging patterns and
701 implications. *Nat. Rev. Genet.* **13**, 97-109 (2012).
- 702 6. Vogt, G. Facilitation of environmental adaptation and evolution by epigenetic
703 phenotype variation: insights from clonal, invasive, polyploid, and domesticated
704 animals. *Environ Epigenet* **3**, dvx002-dvx002 (2017).
- 705 7. Dixon, G. B., Bay, L. K. & Matz, M. V. Bimodal signatures of germline methylation
706 are linked with gene expression plasticity in the coral *Acropora millepora*. *BMC*
707 *Genomics* **15**, 1109 (2014).
- 708 8. Dimond, J. L. & Roberts, S. B. Germline DNA methylation in reef corals: patterns
709 and potential roles in response to environmental change. *Mol. Ecol.* (2015).
- 710 9. Putnam, H. M., Davidson, J. M. & Gates, R. D. Ocean acidification influences host
711 DNA methylation and phenotypic plasticity in environmentally susceptible corals.
712 *Evol. Appl.* **9**, 1165-1178 (2016).
- 713 10. Dixon, G. B., Bay, L. K. & Matz, M. V. Evolutionary Consequences of DNA
714 Methylation in a Basal Metazoan. *Mol. Biol. Evol.* **33**, 2285-2293 (2016).
- 715 11. Neri, F. *et al.* Infragenic DNA methylation prevents spurious transcription initiation.
716 *Nature* **543**, 72-77 (2017).
- 717 12. Tambutte, E. *et al.* Morphological plasticity of the coral skeleton under CO₂-driven
718 seawater acidification. *Nat. Commun.* **6**, 7368 (2015).
- 719 13. Venn, A. A. *et al.* Impact of seawater acidification on pH at the tissue-skeleton
720 interface and calcification in reef corals. *Proc. Natl. Acad. Sci. U S A* **110**, 1634-1639
721 (2013).

722 14. Lyko, F. *et al.* The honey bee epigenomes: differential methylation of brain DNA in
723 queens and workers. *PLoS Biol* **8**, e1000506 (2010).

724 15. Wang, X. *et al.* Function and evolution of DNA methylation in *Nasonia vitripennis*.
725 *PLoS Genet*. **9**, e1003872 (2013).

726 16. Zemach, A., McDaniel, I. E., Silva, P. & Zilberman, D. Genome-wide evolutionary
727 analysis of eukaryotic DNA methylation. *Science* **328**, 916-919 (2010).

728 17. Huh, I., Zeng, J., Park, T. & Yi, S. V. DNA methylation and transcriptional noise.
729 *Epigenetics Chromatin* **6**, 9 (2013).

730 18. Varley, K. E. *et al.* Dynamic DNA methylation across diverse human cell lines and
731 tissues. *Genome Res*. **23**, 555-567 (2013).

732 19. Fine, M. & Tchernov, D. Scleractinian coral species survive and recover from
733 decalcification. *Science* **315**, 1811 (2007).

734 20. Ries, J. B., Cohen, A. L. & McCorkle, D. C. A nonlinear calcification response to
735 CO₂-induced ocean acidification by the coral *Oculina arbuscula*. *Coral Reefs* **29**, 661-
736 674 (2010).

737 21. Kvitt, H. *et al.* Breakdown of coral colonial form under reduced pH conditions is
738 initiated in polyps and mediated through apoptosis. *Proc. Natl. Acad. Sci. U S A* **112**,
739 2082-2086 (2015).

740 22. Su, K. H. *et al.* HSF1 critically attunes proteotoxic stress sensing by mTORC1 to
741 combat stress and promote growth. *Nat. Cell Biol*. **18**, 527-539 (2016).

742 23. Wang, M. C., Bohmann, D. & Jasper, H. JNK extends life span and limits growth by
743 antagonizing cellular and organism-wide responses to insulin signaling. *Cell* **121**,
744 115-125 (2005).

745 24. Inoue, D., Ohe, M., Kanemori, Y., Nobui, T. & Sagata, N. A direct link of the Mos-
746 MAPK pathway to Erp1/Emi2 in meiotic arrest of *Xenopus laevis* eggs. *Nature* **446**,
747 1100-1104 (2007).

748 25. Tamura, R. E. *et al.* GADD45 proteins: central players in tumorigenesis. *Curr. Mol.*
749 *Med*. **12**, 634-651 (2012).

750 26. Coleman, M. L., Marshall, C. J. & Olson, M. F. RAS and RHO GTPases in G1-phase
751 cell-cycle regulation. *Nat. Rev. Mol. Cell Biol*. **5**, 355-366 (2004).

752 27. Moya, A. *et al.* Rapid acclimation of juvenile corals to CO₂ -mediated acidification
753 by upregulation of heat shock protein and Bcl-2 genes. *Mol. Ecol*. **24**, 438-452 (2015).

754 28. Ganot, P. *et al.* Structural molecular components of septate junctions in cnidarians
755 point to the origin of epithelial junctions in eukaryotes. *Mol. Biol. Evol*. **32**, 44-62
756 (2015).

757 29. Chadwick, N. E. & Morrow, K. M. in *Coral Reefs: An Ecosystem in Transition* (eds
758 Zvy Dubinsky & Noga Stambler) 347-371 (Springer Netherlands, 2011).

759 30. Mascarelli, A. Climate-change adaptation: Designer reefs. *Nature* **508**, 444-446
760 (2014).

761 31. Schubeler, D. Function and information content of DNA methylation. *Nature* **517**,
762 321-326 (2015).

763 32. Moya, A. *et al.* Carbonic anhydrase in the scleractinian coral *Stylophora pistillata*:
764 characterization, localization, and role in biomineralization. *J. Biol. Chem*. **283**,
765 25475-25484 (2008).

766 33. Kaniewska, P. *et al.* Transcriptomic Changes in Coral Holobionts Provide Insights
767 into Physiological Challenges of Future Climate and Ocean Change. *PLoS One* **10**,
768 e0139223 (2015).

769 34. Vidal-Dupiol, J. *et al.* Genes related to ion-transport and energy production are
770 upregulated in response to CO₂-driven pH decrease in corals: new insights from
771 transcriptome analysis. *PLoS One* **8**, e58652 (2013).

772 35. Zoccola, D. *et al.* Bicarbonate transporters in corals point towards a key step in the
773 evolution of cnidarian calcification. *Sci. Rep.* **5**, 9983 (2015).

774 36. Drake, J. L. *et al.* Proteomic analysis of skeletal organic matrix from the stony coral
775 *Stylophora pistillata*. *Proc. Natl. Acad. Sci. U S A* **110**, 3788-3793 (2013).

776 37. Mass, T. *et al.* Temporal and spatial expression patterns of biomineralization proteins
777 during early development in the stony coral *Pocillopora damicornis*. *Proc. Biol. Sci.*
778 **283** (2016).

779 38. Brooks, J. M. & Wessel, G. M. The major yolk protein in sea urchins is a transferrin-
780 like, iron binding protein. *Dev. Biol.* **245**, 1-12 (2002).

781 39. Reef, R., Kaniewska, P. & Hoegh-Guldberg, O. Coral skeletons defend against
782 ultraviolet radiation. *PLoS One* **4**, e7995 (2009).

783 40. Hwang, S. P., Partin, J. S. & Lennarz, W. J. Characterization of a homolog of human
784 bone morphogenetic protein 1 in the embryo of the sea urchin, *Strongylocentrotus*
785 *purpuratus*. *Development* **120**, 559-568 (1994).

786 41. Martin, M. Cutadapt removes adapter sequences from high-throughput sequencing
787 reads. *EMBnet.journal* **17**, pp. 10-12 (2011).

788 42. Krueger, F. & Andrews, S. R. Bismark: a flexible aligner and methylation caller for
789 Bisulfite-Seq applications. *Bioinformatics* **27**, 1571-1572 (2011).

790 43. Macmanes, M. D. On the optimal trimming of high-throughput mRNA sequence data.
791 *Front. Genet.* **5**, 13 (2014).

792 44. Bray, N. L., Pimentel, H., Melsted, P. & Pachter, L. Near-optimal probabilistic RNA-
793 seq quantification. *Nat. Biotechnol.* (2016).

794 45. Pimentel, H., Bray, N. L., Puente, S., Melsted, P. & Pachter, L. Differential analysis
795 of RNA-seq incorporating quantification uncertainty. *Nat. Methods* (2017).

796 46. Kim, D., Langmead, B. & Salzberg, S. L. HISAT: a fast spliced aligner with low
797 memory requirements. *Nat. Methods* **12**, 357-360 (2015).

798 47. Alexa, A., Rahnenfahrer, J. & Lengauer, T. Improved scoring of functional groups
799 from gene expression data by decorrelating GO graph structure. *Bioinformatics* **22**,
800 1600-1607 (2006).

801 48. Bustin, S. A. *et al.* The MIQE guidelines: minimum information for publication of
802 quantitative real-time PCR experiments. *Clin. Chem.* **55**, 611-622 (2009).

803 49. Untergasser, A. *et al.* Primer3--new capabilities and interfaces. *Nucleic Acids Res.* **40**,
804 e115 (2012).

805 50. Puverel, S. *et al.* Soluble organic matrix of two Scleractinian corals: partial and
806 comparative analysis. *Comp. Biochem. Physiol. B Biochem. Mol. Biol.* **141**, 480-487
807 (2005).

808